Ground State Properties of Uranium Isotope Chain: A Relativistic Mean Field Approach

Di Xu[1] and Hongfei Zhang[1,2,*]

[1]School of Physics, Xi'an Jiaotong University, 710049 Xi'an, People's Republic of China
[2]School of Nuclear Science and Technology, Lanzhou University, 730000 Lanzhou, People's Republic of China

The study of uranium isotopes plays a crucial role in advancing our knowledge of nuclear physics, particularly in the realms of isospin and exotic nuclei. This research focuses on the ground-state properties of uranium isotopes ranging from A = 203 to A = 305. Key physical quantities examined include binding energy, quadrupole deformation, isotopic displacement, single-particle energy levels, and nucleon density distributions. Recent experimental advancements in uranium isotope studies emphasize the indispensable role of theoretical models in interpreting experimental data. Moreover, the industrial applications of uranium—especially in nuclear energy production and weapons development—underscore its importance and the necessity for accurate theoretical insights. The Framework of the Finite-Range Droplet Model (FRDM model) has been utilized for comparative analysis, as its predictions closely align with experimental results. Through an analysis of single-particle energy levels and continuous state occupancy, this study identifies ^{207}U as the proton drip line nucleus. This research not only deepens our understanding of uranium isotopes but also provides a solid theoretical foundation to guide future experimental investigations.

Keywords: Relativistic Mean Field, BCS Theory, Uranium Isotopic Chain

I. INTRODUCTION

The exploration of the mass and charge limits of atomic nuclei is one of the fundamental challenges in nuclear physics. With advancements in heavy ion accelerators and advanced detection systems, the synthesis of new superheavy elements, such as element 119 following the discovery of element 118, has gained significant attention [1–6]. These efforts are crucial not only for extending the periodic table but also for deepening our understanding of nuclear shell structure. The stability of heavy elements is intricately linked to the arrangement of protons and neutrons, and many nuclear structure theories, from the shell model proposed by Mayer and Jensen [7] to modern microscopic approaches, have sought to predict these configurations, particularly the so-called magic numbers.

A key element in the study of nuclear structure is the concept of "magic numbers". Magic numbers are specific numbers of nucleons (protons or neutrons) that result in highly stable atomic nuclei due to closed shells in the nuclear structure, analogous to electron shells in atoms. Historically, the classic magic numbers were identified as 2, 8, 20, 28, 50, 82, and 126. However, recent theoretical advances and experimental observations have revealed the existence of new magic numbers, particularly in the superheavy region and among exotic nuclei. For example, various nuclear models, such as the Skyrme-Hartree-Fock and the relativistic continuum Hartree-Bogoliubov models [8], predict different sets of magic numbers beyond the traditional ones. These include proton numbers Z = 114, 120, and 126, and neutron numbers N = 172, 184, and 198 [9, 10], which are expected to provide enhanced stability for superheavy nuclei. Moreover, recent research by Rydin [11] has suggested additional magic numbers based on a geometrical packing approach, which implies new magic numbers such as Z = 90, 100, and 118, as well as neutron numbers like N = 58, 68, and 76. These findings indicate that the magic number landscape is far more nuanced than previously thought, and the concept of magicity continues to evolve as new experimental data becomes available.

Recently, the study of uranium isotopes has played an essential role in both theoretical and applied nuclear physics. Uranium is pivotal to nuclear energy and weapons applications, while also serving as a potential starting point for synthesizing superheavy nuclei [12] through nuclear decay pathways. The understanding of the uranium isotope chain, particularly in terms of ground-state properties such as binding energy, deformation, and density distributions, provides insights into the broader aspects of nuclear stability and shell structure.

Recent experimental advancements have significantly contributed to the study of uranium isotopes, particularly through the synthesis and characterization of new neutron-deficient isotopes such as ^{215}U. In 2015, the new isotope ^{215}U was produced using a complete fusion reaction involving ^{180}W and ^{40}Ar, followed by the separation of evaporation residues using the gas-filled recoil separator SHANS. The identification of ^{215}U was based on energy-position-time correlations, with an observed -particle energy of 8.428 MeV and a half-life of approximately 0.73 ms [13]. Similarly, experiments have determined the properties of Uranium, showing a consistent trend in the α-decay behavior of neutron-deficient uranium isotopes [14]. These experimental efforts, aided by facilities like the Heavy Ion Research Facility in Lanzhou (HIRFL), provide essential data that validates theoretical predictions and extends our knowledge of the stability and decay characteristics of heavy nuclei [15].

Theoretical advancements in nuclear physics have led to the development of several models to describe atomic nuclei, including first-principle methods [16–18], the shell model [19–22], and density functional theory (DFT) [23, 24]. Among these, the Relativistic Mean Field (RMF) theory, a variant of DFT, has proven to be a powerful tool in describing nuclear structure. RMF theory incorporates relativistic effects, providing a more comprehensive description of nucleon

* zhanghongfei@lzu.edu.cn

interactions and allowing for the prediction of ground state properties and magic numbers with notable accuracy. Previous studies have shown that RMF theory, combined with the BCS approach to treat pairing correlations [25, 26], is effective in describing the ground state properties of isotopes near the proton drip line.

Despite these advances, several challenges remain in understanding the complete behavior of uranium isotopes, particularly those near the proton drip line, where conventional models face difficulties due to the intricate interplay of pairing forces and continuum effects. In this study, we employ the RMF theory framework, utilizing the TM1 parameter set, to systematically investigate the ground state properties of uranium isotopes ranging from A = 204 to A = 305. Our work aims to provide new insights into binding energies, deformation characteristics, and proton drip line behavior by comparing RMF results with the Finite-Range Droplet Model (FRDM) [27, 28] predictions.

This paper is organized as follows: In Section II, we provide a brief overview of the RMF theory and its application in our study. Section III presents our analysis of the ground state properties of uranium isotopes. Section IV discusses the identification of the proton drip line nucleus within the uranium chain. Finally, in Section V, we summarize the results and their implications for future experimental and theoretical studies in the field.

II. METHODOLOGY AND THEORETICAL FRAMEWORK

A. RELATIVISTIC MEAN FIELDS

We have used the Lagrangian density

$$\begin{aligned}\mathcal{L} = &\bar{\psi}_i\{i\gamma^\mu\partial_\mu - M\}\psi_i \\ &+ \frac{1}{2}\partial^\mu\sigma\partial_\mu\sigma - U(\sigma) - \mathrm{g}_\sigma\overline{\psi}_i\psi_i\sigma \\ &- \frac{1}{4}\Omega^{\mu\nu}\Omega_{\mu\nu} + \frac{1}{2}m_\omega^2\omega^\mu\omega_\mu - \mathrm{g}_\omega\overline{\psi}_i\gamma^\mu\psi_i\omega_\mu \\ &- \frac{1}{4}\vec{R}^{\mu\nu}\vec{R}_{\mu\nu} + \frac{1}{2}m_\rho^2\vec{\rho}^\mu\vec{\rho}_\mu - \mathrm{g}_\rho\overline{\psi}_i\gamma^\mu\vec{\tau}\psi_i\vec{\rho}_\mu \\ &- \frac{1}{4}F^{\mu\nu}F_{\mu\nu} - e\overline{\psi}_i\gamma^\mu\frac{(1+\tau_3)}{2}\psi_i A_\mu\end{aligned} \tag{1}$$

The first row of nucleon terms, ψ_i, is the wave function of a nucleon where i represents a nucleon inside a nucleus. The next three terms are the σ meson, ω meson, and ρ meson terms. M, m_σ, m_ρ, and m_ω are the masses of the nucleus and the three mesons, respectively. g_σ, g_ω, and g_ρ are the coupling constants for the three mesons, respectively. The value of the nonlinear potential $U(\sigma)$ for the σ term [29] and the values of the meson field and electromagnetic field tensor are as follows.

$$U(\sigma) = \frac{1}{2}m_\sigma\sigma^2 + \frac{1}{3}g_2\sigma^3 + \frac{1}{4}g_3\sigma^4, \tag{2}$$

$$\begin{aligned}\Omega^{\mu\nu} &= \partial^\mu\omega^\nu - \partial^\nu\omega^\mu, \\ R^{\mu\nu} &= \partial^\mu\rho^\nu - \partial^\nu\rho^\mu, \\ F^{\mu\nu} &= \partial^\mu A^\nu - \partial^\nu A^\mu.\end{aligned} \tag{3}$$

The Dirac equation and Klein-Gordon equations are derived from the Lagrangian density by applying the variational method. For the numerical solution of these equations, the axially symmetric harmonic oscillator is used as a basis for expanding the wave function in cylindrical coordinates, allowing the effective treatment of deformed nuclei. Initially, trial calculations were performed using $N_f = N_b = 12$ for the selection of the major shell components representing the number of oscillator shells for fermions and bosons.To improve the accuracy of the results, the model parameters were later refined to $N_f = N_b = 20$ and the the iteration limit was set to 1600, the error value was 10^{-7} ,which ensures more precise representation of the nucleon wave functions, especially in the context of deformed nuclear systems.

To further enhance the analysis, three parameter sets, NL1, TM1, and NLSH, are utilized in this study. Each set provides different values for the coupling constants and meson masses, affecting the representation of nuclear interactions and, consequently, the nuclear structure predictions. Specifically, the TM1 parameter set, widely acknowledged for its effectiveness in ground-state property calculations, was chosen as the primary model for most calculations presented in this work.For investigations near the proton drip line, comparisons were made among the NL1, TM1, and NLSH sets to assess their respective accuracy and consistency in predicting the properties of exotic nuclei. The parameters for each set are listed below [29–31]:

Parameter	TM1	NL1	NLSH
m_σ (MeV)	511.198	492.25	526.059
m_ω (MeV)	783.0	795.36	783.0
m_ρ (MeV)	770.0	763.0	763.0
g_σ	10.0289	10.138	10.4434
g_ω	12.6139	13.285	12.945
g_ρ	4.6322	4.975	4.382
b	-7.2325 $\times 10^{-4}$	-6.9099 $\times 10^{-4}$	-6.9099$\times 10^{-4}$
c	0.6183	-5.4965 $\times 10^{-5}$	0.615

TABLE 1. Parameter sets used in the RMF model: TM1, NL1, and NLSH.

B. ground-state properties

In the following, we will outline the methods used to calculate several important nuclear properties, including binding energy, quadrupole deformation, continuum occupation numbers (or single-particle energy levels), and nucleon density distributions. The relationships and formulas used are derived from the referenced study by Gambhir et al. (1990) [32]. These calculations provide comprehensive insights into the ground-state characteristics of uranium isotopes.

The average binding energy, an essential quantity in determining nuclear stability, is obtained by integrating the energy densities of the nucleons and meson fields. The total binding energy is expressed as:

$$
\begin{aligned}
E(\psi_i^\dagger, \psi_i, \sigma, \omega^0, \rho^0, A^0, v_i) &= E_{\text{part}} + E_\sigma + E_\omega + E_\rho \\
&+ E_\epsilon + E_{\text{pair}} + E_{\text{CM}} - AM,
\end{aligned} \tag{4}
$$

Here, E_{part} represents the kinetic energy of the nucleons. E_σ, E_ω and E_ρ represent the contributions from the interactions mediated by the scalar meson field (σ meson), the vector meson field (ω meson), and the isovector-vector meson field (ρ meson), respectively, which are responsible for the effective nuclear force between nucleons. E_c refers to the Coulomb energy, accounting for the electrostatic repulsion between protons. E_{pair} describes the pairing energy between nucleons, which is particularly important for maintaining nuclear stability by minimizing the total energy. E_{AM} refers to the center-of-mass correction energy, which ensures the accuracy of the calculation by correcting for the spurious motion of the center of mass.

The quadrupole deformation parameter was determined to quantify the shape of the nuclei. This deformation parameter is calculated based on the quadrupole moment of the nucleus:

$$
Q = Q_n + Q_p = \sqrt{\frac{16\pi}{5}} \frac{3}{4\pi} A R_0^2 \beta, \tag{5}
$$

where $R_0 = 1.2A^{1/3}$(fm). And the quadrupole moments are calculated by using the expressions:

$$
Q_{n,p} = \langle 2r^2 P_2(\cos\theta) \rangle_{n,p} = \langle 2z^2 - x^2 - y^2 \rangle_{n,p} \tag{6}
$$

For single-particle energy levels and continuum occupation numbers, we used the BCS approach to account for pairing correlations. The occupation number for each single-particle state is given by:

$$
n_i = v_i^2 = \frac{1}{2}\left(1 - \frac{\epsilon_i - \lambda}{\sqrt{(\epsilon_i - \lambda)^2 + \Delta^2}}\right) \tag{7}
$$

ϵ_i represents the single-particle energy of a specific state i. λ is the chemical potential ensuring particle number conservation, Δ and is the pairing gap, which quantifies the strength of the pairing interaction between nucleons, such as paired neutrons or protons.The coefficients μ_i and v_i denote the probability amplitudes for a single-particle state i to be occupied or unoccupied, respectively, and they satisfy $\mu_i^2 + v_i^2 = 1$.

RMF theory is an effective framework for describing nuclear structure by considering the interactions between nucleons mediated by various mesons. However, it alone does not fully account for the pairing interactions between nucleons, which play a significant role in determining the stability and deformation properties of nuclei, particularly those in open-shell configurations. To address this, the BCS theory [32, 33] is employed as it allows for the effective treatment of these pairing correlations, providing a more complete and accurate depiction of nuclear ground state properties. This is especially important for heavy elements like uranium, where pairing interactions influence many key properties, such as binding energy and deformation.

Many properties of the nucleus exhibit parity dependence, leading to distinct pair correlations between protons and neutrons. The RMF approach used here includes these pair interactions by employing the BCS theory as a perturbative correction, specifically incorporating effective pair force constants for protons and neutrons given by:

$$
\begin{aligned}
G_n &= \frac{21}{A}\left(1 - \frac{N-P}{2A}\right) \\
G_p &= \frac{27}{A}\left(1 + \frac{N-P}{2A}\right)
\end{aligned} \tag{8}
$$

where A is the mass number, and N and P represent the neutron and proton numbers, respectively. Also if in systems with an odd number of nucleons, there is one nucleon that remains unpaired, which can significantly affect the pairing correlations. So the blocking method is an important complementary technique used when dealing with this case of odd-A nuclei, which ensures that this unpaired nucleon is "frozen" in its specific orbital, characterized by an energy level ϵ_k thus preventing it from participating in the overall pairing interaction [34].

Thus, the integration of BCS theory, blocking method, and RMF theory forms a comprehensive framework for studying uranium isotopes. These methods together allow for accurate calculations of pairing interactions, single-particle energies, and deformation parameters, which are essential for understanding both the stability and the structural nuances of heavy nuclei, including those near the proton drip line.

III. DETERMINATION OF THE DRIP-LINE NUCLEUS IN THE U ISOTOPE CHAIN

To determine the proton drip line [35–37], we analyzed the continuum state occupation number of uranium isotopes calculated with different relativistic mean-field parameters: NL1, TM1, and NLSH. As depicted in Fig. 1, the continuum state occupation number shows distinct behavior for the different parameter sets.For isotopes with mass numbers ranging from $A = 203$ to $A = 305$, the occupation number generally remains low for mid-range isotopes, indicating bound systems. However, as seen in the figure, each parameter set predicts a different mass number as the proton drip-line nucleus. Specifically, the NL1 parameter set identifies $A = 210$ as the proton drip-line nucleus, while the TM1 and NLSH parameter sets predict the proton drip lines at $A = 206$ and $A = 208$, respectively. These differences highlight the sensitivity of the drip-line prediction to the choice of interaction parameters.

In Figs. 2, the single-particle energy levels near the Fermi surface of the drip-line nuclei and their neighboring isotopes

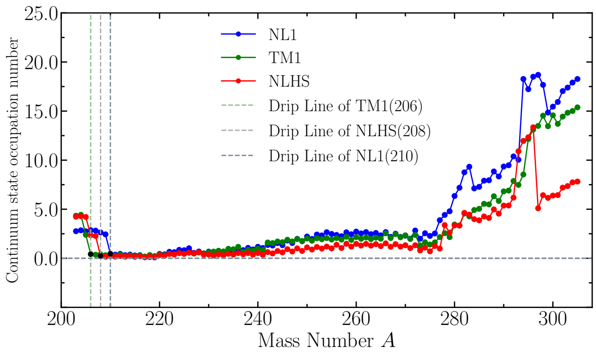

Fig. 1. Continuum state occupation number and drip line of protons.

are displayed for NL1, TM1, and NLSH parameters. These energy level distributions illustrate that for nuclei at the proton drip line, the occupation of continuum states becomes prominent, signifying their unbound nature.Thus the proton drip line kernels for the three parameter sets are ^{209}U(NL1), ^{205}U(TM1), ^{207}U(NLSH). Importantly, the differing results of the three parameter sets reflect the sensitivity of the RMF model to the choice of parameters. In the absence of definitive experimental data, it is advisable to consider the results from multiple parameter sets to form a more representative prediction and acknowledge this uncertainty in the analysis.

As describing the region of nuclei with relatively more protons along the isotopic chain applying the better parameter set NLSH, we consider here the proton dripline nuclei as a result of the calculation of the NLHS parameter set ^{207}U. For the NLHS parameter set, the analysis of ^{207}U and ^{208}U reveals significant details regarding the occupation of energy states near the Fermi surface. In ^{207}U, the first positive-energy state above the Fermi surface, identified as $\frac{1}{2}^+$, has an energy of 1.32 MeV and an occupation probability of 30.8%. This suggests that a substantial fraction of protons occupy an unbound state, indicating that ^{207}U is at the proton drip line for the NLSH parameter set. Conversely, for ^{208}U, the last proton resides in a negative-energy state, and the first positive-energy state above the Fermi surface shows zero occupancy and occupation probability. This clearly highlights the difference in binding behavior between ^{207}U and ^{208}U, confirming that ^{207}U lies on the proton drip line, whereas ^{208}U remains bound and stable. This analysis provides further evidence of the NLSH parameter set's balanced approach in predicting the proton drip line by accurately capturing the transition between bound and unbound states.

As the occupation number of the continuum state fluctuates significantly on the neutron-rich side of the uranium isotopic chain, a distinct anomaly is observed when compared to the proton side. This anomaly is particularly evident at mass numbers $A = 277$ and $A = 278$, where the continuum occupation number exhibits an abrupt change from 0.99 to 3.38. This step-like transition suggests that the mean-field strength and pairing correlation strength are comparable in magnitude for these nuclei. In such cases, treating pairing correlations merely as a perturbation is no longer valid, since their contribution is significant enough to influence the nucleon dynamics substantially. Consequently, pairing correlations must be rigorously included in the self-consistent equations of motion rather than as a small correction.

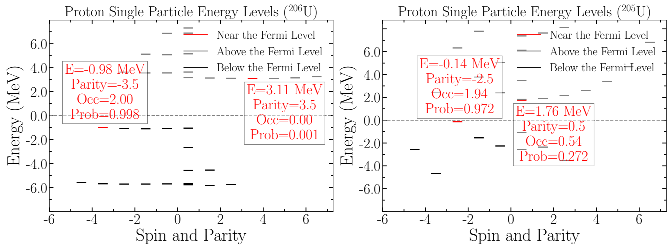

(a) Single-particle energy levels of ^{205}U and ^{206}U for TM1

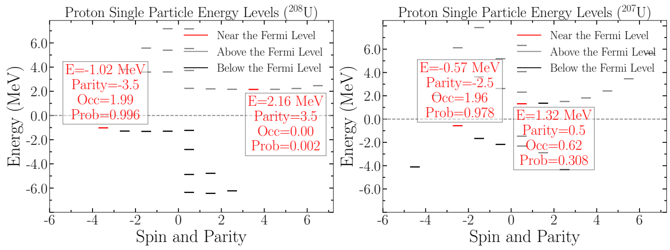

(b) Single-particle energy levels of ^{207}U and ^{208}U for NLSH

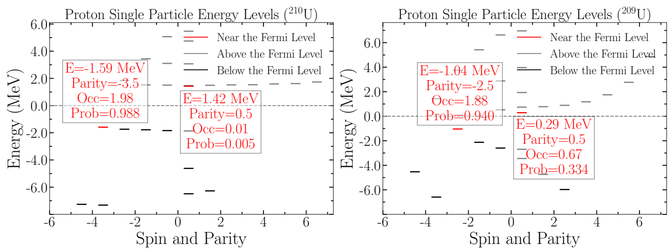

(c) Single-particle energy levels of ^{209}U and ^{210}U for NL1

Fig. 2. Energy levels near the Fermi surface of the drip-line nuclei for NL1, TM1, and NLSH parameters.

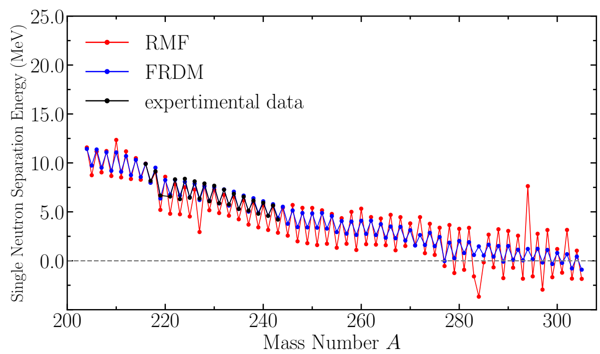

Fig. 3. One-neutron separation energy S_n of U isotope chains.

The improper perturbative treatment of these pairing effects leaves some neutron-rich nuclei in a state where the last neutrons occupy continuum levels, which is unphysical under

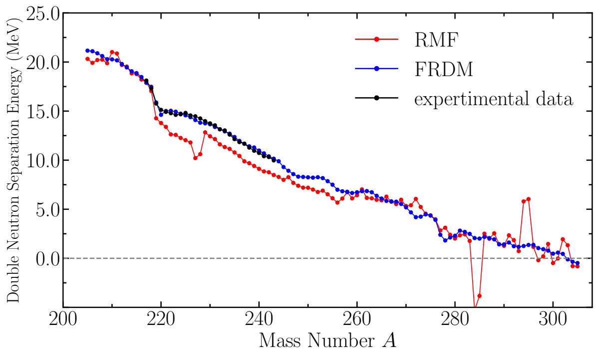

Fig. 4. Two-neutron separation energy $S_{2\mathrm{n}}$ of U isotope chains.

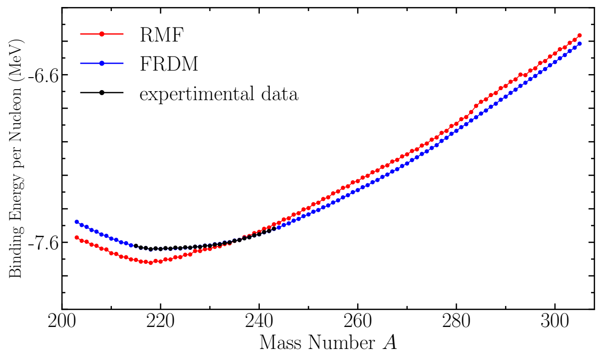

Fig. 5. Binding Energy per Nucleon.

these conditions and results in an incorrect representation of the nucleus's binding properties.The presence of nuclei occupying continuum states in this region implies that the pairing correlations should be inherently included in the mean-field framework, as these correlations are essential in stabilizing the nuclear system and determining the drip line. Therefore, the sharp increase in the continuum occupation number at $A = 277$ and $A = 278$ cannot be interpreted accurately without incorporating these pairing correlations self-consistently.

To further clarify the determination of the neutron drip line, we also analyzed the one-neutron separation energy S_n and the two-neutron separation energy S_{2n}, as shown in Figs. 3 and 4. The experimental data were sourced from [38]. The results indicate that, up to the last nuclei in the uranium chain, neither the one-neutron nor the two-neutron separation energy exhibits a clear trend towards zero, which would signify the drip line. Instead, the separation energies decrease gradually without reaching a definitive cut-off, implying that these nuclei are still marginally bound. This lack of a clear zero-crossing in the separation energies suggests that using the S_n and S_{2n} values alone is also insufficient for precisely identifying the neutron drip line.

IV. PROPERTIES OF THE GROUND STATE OF NUCLEI IN THE U ISOTOPE CHAIN

The results of the average binding energy are depicted in Fig. 5. It is evident that our calculations are in good agreement with the Finite-Range Droplet Model (FRDM) data, with the lowest binding energy observed at the neutron magic number $N = 126$. This agreement indicates that our chosen force constants, the treatment of pairing correlations, and the implementation of the blocking method for $odd - A$ nuclei provide a reliable theoretical framework. Furthermore, our results show that at $N = 126$ (corresponding to ^{218}U) [39], the average binding energy reaches its maximum value. The binding energy of ^{218}U calculated with our approach is notably higher than that predicted by the FRDM, suggesting an enhanced representativeness of our model.

The deformation of the uranium isotope chain is presented in Fig. 6. The red line represents the Finite-Range Droplet Model (FRDM) predictions, while the black line corresponds to the Relativistic Mean Field (RMF) calculations. A comparison reveals that, unlike the FRDM results, the RMF model shows a smoother deformation [40] trend without the abrupt changes seen at mass numbers $A = 284 - 296$ This smoother trend suggests that the RMF approach provides a more consistent representation for the quadrupole deformation, particularly in regions where spherical symmetry is expected. Additionally, the deformation pattern indicates that nuclei with mass numbers less than $A = 208$ exhibit a prolate, elongated ellipsoidal shape, while those between $A = 208 - 228$ are almost spherical, exhibiting very small deformations. Beyond $A = 228$, the deformation alternates between prolate and spherical, except for $A = 256$, where the deformation suddenly reduces to a spherical shape. Throughout the isotopic chain, there are no pronounced oblate, flat ellipsoidal shapes, and the few negative deformation values can be interpreted as spheroidal, rather than strongly oblate, shapes.

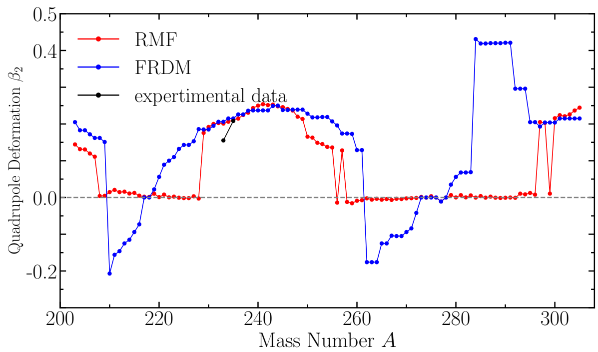

Fig. 6. Deformation of nuclei in a chain of uranium isotopes for 20 shells.

Using ^{218}U, a semimagic nucleus, as the reference, we analyzed the isotope shifts presented in Fig. 7. The data exhibit a generally smooth increase, with a noticeable flattening for nuclei with mass numbers $A = 247$ to $A = 256$. In nuclear physics, a "kink" in isotope shift data refers to an abrupt change in the trend of nuclear charge radii as a function of neutron number, typically occurring at neutron magic numbers. This phenomenon has been observed in rare-earth ele-

ments, where such kinks appear near neutron magic numbers, indicating changes in nuclear structure and stability [39, 41–46]

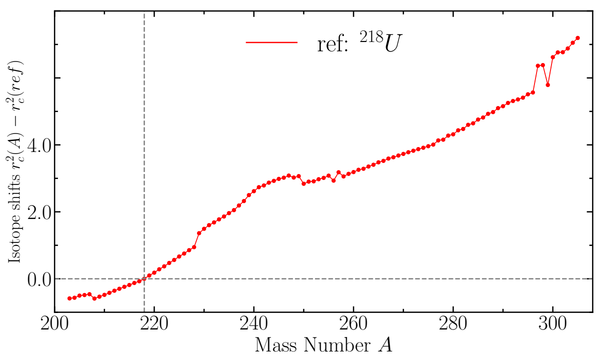

Fig. 7. the Isotope shifts $r_c^2(A) - r_c^2(ref)$ for the U isotope chain.

However, in our study of uranium isotopes, no evident kink is observed at $A = 218$, corresponding to the neutron magic number $N = 126$. This absence suggests that the expected shell closure effect at $N = 126$ does not manifest prominently in the isotope shift data for uranium. Consequently, based on isotope shift analysis alone, we cannot confirm $A = 218$ as a magic number nucleus. This finding aligns with similar research [47, 48], indicating that the manifestation of magic numbers can vary across different elements and isotopic chains.

The analysis of neutron and proton density distributions along the major axis for uranium isotopes, including ^{205}U, ^{206}U, and ^{238}U, provides important insights into their structural characteristics and deformation properties.

First, the density distributions of protons and neutrons are generally centered around the nucleus, with a distinct peak in density near the core. In all isotopes analyzed, the neutron density extends further than the proton density, indicating the presence of a "neutron skin." This neutron skin, where the neutrons dominate the outer regions of the nucleus, is a common feature for neutron-rich heavy nuclei and contributes to the enhanced stability observed in these uranium isotopes. The proton density, on the other hand, is more concentrated towards the center, which reflects the influence of Coulomb repulsion pushing protons inward to counterbalance their mutual repulsion forces.

Among the isotopes, ^{205}U displays the smallest deformation, suggesting a nearly spherical shape, while ^{238}U exhibits the largest deformation, characterized by significant elongation along the major axis. ^{238}U show intermediate deformations, which can be described as prolate, resembling elongated ellipsoids. The neutron skins in these nuclei become more pronounced as the mass number increases, which aligns with the increasing neutron-to-proton ratio [49].

These findings collectively emphasize the significance of neutron excess and nuclear deformation in determining the density profiles of uranium isotopes. The presence of neutron skins in all the analyzed isotopes indicates that neutrons dominate the periphery of these nuclei, which has important implications for understanding nuclear stability, interaction cross-sections, and the behavior of these nuclei near the dripline. The RMF theory effectively captures these differences in density distributions and provides a comprehensive picture of the underlying nuclear structure of heavy isotopes, contributing to a better understanding of their stability and deformation characteristics.

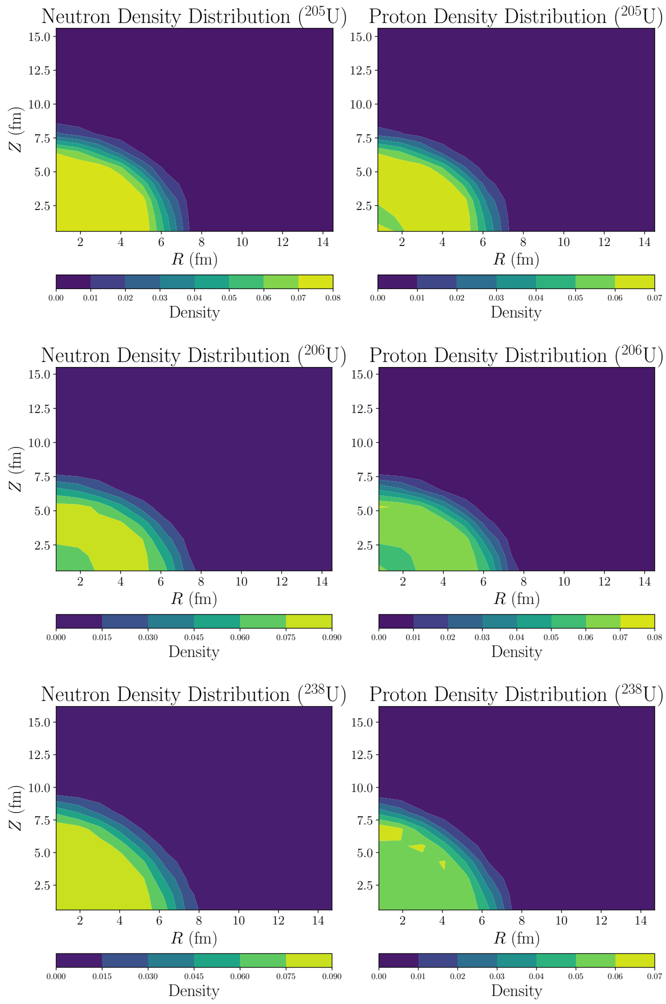

Fig. 8. Density distribution of neutrons and protons.

V. SUMMARY

We have calculated the ground state properties of nuclei in the uranium isotope chain using relativistic mean-field (RMF) theory, incorporating pairing correlations through the Bardeen-Cooper-Schrieffer (BCS) approach. Our results, which show good agreement with the Finite-Range Droplet Model (FRDM) data, particularly at the neutron magic number $N = 126$ validate the robustness of our approach in modeling the binding energies and deformation properties of uranium isotopes. By analyzing the Fermi surface and single-particle energy levels, we confirmed that ^{207}U is a proton

dripline nucleus due to its continuum state proton occupancy, while ^{208}U remains bound, highlighting the precise identification of the dripline.

In the future, the continued development of RMF theory, incorporating more advanced treatments of pairing and beyond-mean-field effects, holds great promise for understanding the properties of nuclei near the dripline, particularly for superheavy elements.Improved predictive models are crucial for practical applications, especially in nuclear fission processes relevant to energy production and reactor safety. Additionally, advancements in experimental facilities will be key to validating theoretical predictions and exploring new regions of the nuclear chart. The synergy between theoretical advancements and experimental verification will deepen our understanding of nuclear structure, stability, and the broader implications for nuclear technology.

VI. ACKNOWLEDGMENTS

This work is supported by National Natural Science Foundation of China (Grants No. 12175170 and No. 11675066).

[1] Y. T. Oganessian, V. K. Utyonkov, Y. V. Lobanov, F. S. Abdullin, A. N. Polyakov, R. N. Sagaidak, I. V. Shirokovsky, Y. S. Tsyganov, A. A. Voinov, G. G. Gulbekian, S. L. Bogomolov, B. N. Gikal, A. N. Mezentsev, S. Iliev, V. G. Subbotin, A. M. Sukhov, K. Subotic, V. I. Zagrebaev, G. K. Vostokin, M. G. Itkis, K. J. Moody, J. B. Patin, D. A. Shaughnessy, M. A. Stoyer, N. J. Stoyer, P. A. Wilk, J. M. Kenneally, J. H. Landrum, J. F. Wild, and R. W. Lougheed, Phys. Rev. C **74**, 044602 (2006).

[2] N. Wang, E.-G. Zhao, and W. Scheid, Phys. Rev. C **89**, 037601 (2014).

[3] J.-X. Li and H.-F. Zhang, Phys. Rev. C **105**, 054606 (2022).

[4] F. Li, L. Zhu, Z.-H. Wu, X.-B. Yu, J. Su, and C.-C. Guo, Phys. Rev. C **98**, 014618 (2018).

[5] B. M. Kayumov, O. K. Ganiev, A. K. Nasirov, and G. A. Yuldasheva, Phys. Rev. C **105**, 014618 (2022).

[6] B.-S. Cai and C.-X. Yuan, Nuclear Science and Techniques **34**, 204 (2023).

[7] M. G. Mayer, Phys. Rev. **75**, 1969 (1949).

[8] K. Wei, Y.-L. Ye, and Z.-H. Yang, Nuclear Science and Techniques **35**, 216 (2024).

[9] K. Rutz, M. Bender, T. Bürvenich, T. Schilling, P.-G. Reinhard, J. A. Maruhn, and W. Greiner, Phys. Rev. C **56**, 238 (1997).

[10] J. J. Li, J. Margueron, W. H. Long, and N. Van Giai, Physics Letters B **753**, 97 (2016).

[11] R. A. Rydin, Annals of Nuclear Energy **38**, 2356 (2011).

[12] Z. Fengshou, Z. Yuhai, Z. Minghao, T. Na, C. Shihui, L. Jingjing, and C. Wei, Journal of Beijing Normal University(Natural Science) **58**, 392 (2022).

[13] H. B. Yang, Z. Y. Zhang, J. G. Wang, Z. G. Gan, L. Ma, L. Yu, J. Jiang, Y. L. Tian, B. Ding, S. Guo, Y. S. Wang, T. H. Huang, M. D. Sun, K. L. Wang, S. G. Zhou, Z. Z. Ren, X. H. Zhou, H. S. Xu, and G. Q. Xiao, The European Physical Journal A **51**, 88 (2015).

[14] Y.-Y. Xu, D.-X. Zhu, Y.-T. Zou, X.-J. Wu, B. He, and X.-H. Li, Chinese Physics C **46**, 114103 (2022).

[15] X. Zhou, M. Wang, Y.-H. Zhang, X.-H. Zhou, X.-L. Yan, and Y.-M. Xing, Nuclear Science and Techniques **35**, 213 (2024).

[16] G. Hupin, S. Quaglioni, and P. Navratil, in *ND 2016: INTERNATIONAL CONFERENCE ON NUCLEAR DATA FOR SCIENCE AND TECHNOLOGY*, EPJ Web of Conferences, Vol. 146, edited by A. Plompen, F. Hambsch, P. Schillebeeckx, W. Mondelaers, J. Heyse, S. Kopecky, P. Siegler, and S. Oberstedt (2017) international Conference on Nuclear Data for Science and Technology (ND), Bruges, BELGIUM, SEP 11-16, 2016.

[17] G. A. Negoita, J. P. Vary, G. R. Luecke, P. Maris, A. M. Shirokov, I. J. Shin, Y. Kim, E. G. Ng, C. Yang, M. Lockner, and G. M. Prabhu, Phys. Rev. C **99**, 054308 (2019).

[18] P. Navrátil, J. P. Vary, and B. R. Barrett, Phys. Rev. Lett. **84**, 5728 (2000).

[19] E. Caurier, G. Martínez-Pinedo, F. Nowacki, A. Poves, and A. P. Zuker, Rev. Mod. Phys. **77**, 427 (2005).

[20] N. Michel, W. Nazarewicz, and M. Płoszajczak, Phys. Rev. C **70**, 064313 (2004).

[21] B. A. Brown and W. A. Richter, Phys. Rev. C **58**, 2099 (1998).

[22] B. A. Brown and B. H. Wildenthal, Annual Review of Nuclear and Particle Science **38**, 29 (1988).

[23] G. A. Lalazissis and P. Ring, ROMANIAN JOURNAL OF PHYSICS **58**, 1038 (2013).

[24] R. Furnstahl, JOURNAL OF PHYSICS G-NUCLEAR AND PARTICLE PHYSICS **31**, S1357 (2005), workshop on Nuclar Forces and Quantum Many-Body Problem, Inst Nucl Theory, Seattle, WA, OCT 04-08, 2004.

[25] G. Lalazissis and S. Raman, PHYSICAL REVIEW C **58**, 1467 (1998).

[26] J. Xiang, Z. P. Li, J. M. Yao, W. H. Long, P. Ring, and J. Meng, Phys. Rev. C **88**, 057301 (2013).

[27] P. Moeller, W. D. Myers, H. Sagawa, and S. Yoshida, PHYSICAL REVIEW LETTERS **108** (2012), 10.1103/PhysRevLett.108.052501.

[28] P. Möller, A. Sierk, T. Ichikawa, and H. Sagawa, Atomic Data and Nuclear Data Tables **109-110**, 1 (2016).

[29] J. Boguta and A. Bodmer, Nuclear Physics A **292**, 413 (1977).

[30] Y. Sugahara and H. Toki, Nuclear Physics A **579**, 557 (1994).

[31] M. M. Sharma, M. A. Nagarajan, and P. Ring, Physics Letters B **312**, 377 (1993).

[32] Y. K. Gambhir, P. Ring, and A. Thimet, Annals of Physics **198**, 132 (1990).

[33] L. Geng, H. Toki, S. Sugimoto, and J. Meng, Progress of Theoretical Physics **110**, 921 (2003).

[34] S. P. Ring P, "The nuclear many-body problem | SpringerLink,".

[35] G. A. Lalazissis and S. Raman, Phys. Rev. C **58**, 1467 (1998).

[36] D. Vretenar, G. A. Lalazissis, and P. Ring, Phys. Rev. C **57**, 3071 (1998).

[37] J. Dobaczewski, I. Hamamoto, W. Nazarewicz, and J. A. Sheikh, Phys. Rev. Lett. **72**, 981 (1994).

[38] International Atomic Energy Agency (IAEA), "Vcharthtml," [Online; accessed on 15-October-2023].

[39] A. E. Barzakh, D. V. Fedorov, V. S. Ivanov, P. L. Molkanov, F. V. Moroz, S. Y. Orlov, V. N. Panteleev, M. D. Seliverstov,

and Y. M. Volkov, Phys. Rev. C **97**, 014322 (2018).

[40] F. K. McGowan, C. E. Bemis, J. L. C. Ford, W. T. Milner, R. L. Robinson, and P. H. Stelson, Phys. Rev. Lett. **27**, 1741 (1971).

[41] G. Lalazissis, M. Sharma, and P. Ring, Nuclear Physics A **597**, 35 (1996).

[42] T. Naito, T. Oishi, H. Sagawa, and Z. Wang, Phys. Rev. C **107**, 054307 (2023).

[43] P. M. Goddard, P. D. Stevenson, and A. Rios, Phys. Rev. Lett. **110**, 032503 (2013).

[44] H. Nakada and T. Inakura, Phys. Rev. C **91**, 021302 (2015).

[45] H. Nakada, Phys. Rev. C **92**, 044307 (2015).

[46] T. Naito, T. Oishi, H. Sagawa, and Z. Wang, Physical Review C **107**, 54307 (2023).

[47] A. N. Andreyev, D. D. Bogdanov, V. I. Chepigin, A. P. Kabachenko, O. N. Malyshev, R. N. Sagajdak, G. M. Ter-Akopian, and A. V. Yeremin, Zeitschrift für Physik A Hadrons and Nuclei **342**, 123 (1992).

[48] M. Bhuyan, B. Maheshwari, H. A. Kassim, N. Yusof, S. K. Patra, B. V. Carlson, and P. D. Stevenson, Journal of Physics G: Nuclear and Particle Physics **48**, 75105 (2021).

[49] M.-Q. Ding, D.-Q. Fang, and Y.-G. Ma, Nuclear Science and Techniques **35**, 211 (2024).